The current issue and full text archive of this journal is available at
www.emeraldinsight.com/0332-1649.htm

On the use of PML for the computation of leaky modes

An application to microstructured optical fibres

Y. Ould Agha, F. Zolla, A. Nicolet and S. Guenneau
Faculté de Saint-Jérôme, Institut Fresnel, UMR 6133, Aix Marseille Universite, Marseille, France

Abstract

Purpose – The purpose of this paper is to present a complete analysis of leaky modes within a microstructured optical fibre (MOF). Some new numerical results illustrating the versatility and accuracy of our approach are to be given.

Design/methodology/approach – A method involving both finite elements and perfectly matched layer (PML) is proposed.

Findings – A rigorous definition of the leaky modes is proposed that leads to a proof of the validity of the PML approach together with a rule for the choice of the PML parameters.

Originality/value – The choice of parameters associated with the PML are discussed in great detail. The accuracy of the constant of propagation (and especially the imaginary part) are highlighted.

Keywords Optical fibres, Finite element analysis, Perfectly matched layers

Paper type Research paper

1. Introduction

Conventional optical fibres rely on total internal reflection. For this, it is well known that the maximum of the index of the core of a fibre has to be greater than the index of the surrounding dielectric (often called cladding). Nowadays, a new class of fibres – namely the microstructured optical fibres (MOFs) – has received considerable attention from the scientific community since pioneering work demonstrated some of their unexpected and remarkable properties such as endlessly single modedness (Cregan *et al.*, 1999), supercontinuum generation (Ranka *et al.*, 2000), … Now, it turns out that the leaky modes are very sensitive to the variation of the refractive index of fibres and especially via the imaginary part of the effective index as shown for MOFs described in paragraph 3.3. In this paper, we propose a versatile and accurate method allowing to obtain efficiently these modes.

2. Finite element modelling

2.1 Governing equations

Let us consider an open waveguide which is invariant along the z-direction, heterogeneous in the xy-plane (cross-section) and possibly anisotropic. Thus, we assume that two tensor fields ($\underline{\underline{\varepsilon_r}}(x,y)$ and $\underline{\underline{\mu_r}}(x,y)$) are given and we let $Z_0 = \sqrt{\mu_0/\varepsilon_0}$ and $k_0 = \omega/c$. Therefore, the problem of propagation in harmonic regime with a time dependence in $\exp(-i\omega t)$ in such fibres amounts to looking for a couple (β, k_0) and a non-vanishing field $F = (H,E)^{\mathrm{T}}$ which is solution of:

COMPEL: The International Journal for Computation and Mathematics in Electrical and Electronic Engineering
Vol. 27 No. 1, 2008
pp. 95-109

0332-1649
DOI 10.1108/03321640810836672

$$\begin{cases} \mathrm{curl}_\beta H = -i\omega\varepsilon_0 \underline{\underline{\varepsilon_r}} E \\ \mathrm{curl}_\beta E = +i\omega\mu_0 \underline{\underline{\mu_r}} H \end{cases} \tag{1}$$

where $\mathrm{curl}_\beta E(x,y) = \mathrm{curl}\,(E(x,y)\mathrm{e}^{i\beta z})\mathrm{e}^{-i\beta z}$ and where $\mathrm{curl}_\beta H$ is defined in the same way. For a given β, these equations can be seen as an eigenproblem:

$$\mathscr{L}_\beta F = k_0 F, \tag{2}$$

with:

$$\mathscr{L}_\beta := \begin{pmatrix} 0 & -iZ_0^{-1}\underline{\underline{\mu_r}}^{-1}\mathrm{curl}_\beta \\ iZ_0\underline{\underline{\varepsilon_r}}^{-1}\mathrm{curl}_\beta & 0 \end{pmatrix}. \tag{3}$$

Of course, from this latest system of equations two equivalent eigenproblems can be derived:

$$\begin{cases} \underline{\underline{\mu_r}}^{-1}\mathrm{curl}_\beta\,(\underline{\underline{\varepsilon_r}}^{-1}\mathrm{curl}_\beta H) = k_0^2 H \\ \underline{\underline{\varepsilon_r}}^{-1}\mathrm{curl}_\beta\,(\underline{\underline{\mu_r}}^{-1}\mathrm{curl}_\beta E) = k_0^2 E. \end{cases} \tag{4}$$

2.2 Spectral problem

In the literature concerning the fibres, at least three kinds of modes are studied; the guided modes, the leaky modes and the radiative modes. All these modes are governed, of course, by the same formal spectral problem (2) but the functional spaces in which they live are different. For this purpose, we have to define accurately these functional spaces.

Definition 1. We say that (E, H) is a guided mode if the following three conditions are fulfilled:

- $(\beta, \omega) \in (\mathbb{R}^+)^2$
- $(E, H) \neq (0, 0)$
- $(E, H) \in [L^2(\mathbb{R}^2)]^3$.

Definition 2. We say that (E, H) is a leaky mode if we can find a strictly positive real number Γ in order to fulfil the following three conditions:

- $(\beta, \omega) \in \mathbb{C}^+ \times \mathbb{R}^+$, where $\mathbb{C}^+ = \{z \in \mathbb{C};\ \Im m\{z\} > 0, \Re e\{z\} > 0\}$
- $(E, H) \neq (0, 0)$
- $(\mathrm{e}^{-\Gamma R}E, \mathrm{e}^{-\Gamma R}H) \in [L^2(\mathbb{R}^2)]^3$, where $R = \sqrt{x^2 + y^2}$.

Definition 3. We say that (*E*, *H*) is a radiative mode if, for any strictly positive real number Γ the following four conditions are fulfilled:

- $(\beta, \omega) \in (\mathbb{R}^+)^2$
- $(E, H) \neq (0, 0)$
- $(E, H) \notin [L^2(\mathbb{R}^2)]^3$.
- $(e^{-\Gamma R}E, e^{-\Gamma R}H) \in [L^2(\mathbb{R}^2)]^3$, where $R = \sqrt{x^2 + y^2}$.

For the sake of simplicity, in this paragraph, we assume that the fibre is made of isotropic and non-magnetic materials. Moreover, the cladding is supposed to be homogeneous. In other words, for a sufficiently large R_0, the permittivity is constant, $\varepsilon_r(x, y) = \varepsilon_\infty$. In this case, provided that:

$$\varepsilon_{\text{Max}} = \max_{(x,y)\in\mathbb{R}^2/\sqrt{x^2+y^2}<R_0} \varepsilon_r(x, y),$$

is greater than ε_∞ and also that finite energy eigenvectors are considered (Definition 1), the spectrum of the operator $\mathcal{L}_\beta$ consists of a discrete set of eigenvalues belonging to $[\beta^2/\varepsilon_{\text{Max}}; \beta^2/\varepsilon_\infty[$ and of continuous spectrum $[\beta^2/\varepsilon_\infty; +\infty]$ (Zolla *et al.*, 2005). On the other hand, when $\varepsilon_{\text{Max}} < \varepsilon_\infty$, only leaky modes may exist and complex valued propagation constants have to be considered. If we focus our attention only on leaky modes propagating along the increasing *z*, it turns out that $\beta' = \Re e\{\beta\}$ and $\beta'' = \Im m\{\beta\}$ are both positive. Note that, if the first condition is fulfilled, the field (*H*,*E*) cannot be of finite energy. Actually, within the cladding every component of the electromagnetic field is solution of Helmholtz equation, namely:

$$\Delta U + \tilde{k}_\infty^2 U = 0, \tag{5}$$

where *U* is one component of either *E* or *H* and $\tilde{k}_\infty^2 = k_\infty^2\varepsilon_\infty - \beta^2$. The function *U* can be written in cylindrical co-ordinates as a Fourier Bessel expansion:

$$U(x, y) = U_c(\rho, \varphi) = \sum_{n\in\mathbb{Z}} c_n H_n^{(1)}(\tilde{k}_\infty\rho)e^{in\varphi}, \tag{6}$$

where $H_n^{(1)}$ refers to the Hankel function of the first kind of order *n*. This latest function has a well known asymptotic behaviour, namely:

$$H_n^{(1)}(\tilde{k}_\infty\rho) = \sqrt{\frac{2}{\pi\tilde{k}_\infty\rho}}e^{-i(n(\pi/2)+(\pi/4))}e^{i\tilde{k}_\infty\rho} + \mathcal{O}(\rho^{-3/2}), \tag{7}$$

and leads to:

$$U_c(\rho, \varphi) = \sigma(\varphi)\frac{e^{i\tilde{k}'_\infty\rho}}{\sqrt{\rho}}e^{-\tilde{k}''_\infty\rho}, \tag{8}$$

with:

$$\sigma(\varphi) = \sqrt{\frac{2}{\pi \tilde{k}_\infty}}\ \mathrm{e}^{-i\pi/4} \sum_{n \in \mathbb{Z}} c_n \mathrm{e}^{in(\varphi - \pi/2)}, \tag{9}$$

where $\tilde{k}'_\infty = \Re\mathrm{e}\{\tilde{k}_\infty\}$ and $\tilde{k}''_\infty = Jm\{\tilde{k}_\infty\}$. It is therefore of prime importance to know the sign of $\tilde{k}''_\infty$. First of all the outgoing wave condition leads to the positiveness of the real part of $\tilde{k}_\infty$. And if we let $\beta = \beta' + i\beta''$, we deduce:

$$\tilde{k}^2_\infty = k_0^2 \varepsilon_\infty - \beta'^2 + \beta''^2 - 2i\beta'\beta'' \tag{10}$$

As a result we have:

$$\beta'\beta'' = -\tilde{k}'_\infty \tilde{k}''_\infty.$$

Bearing in mind that β' and β'' are both positive together with $\tilde{k}'_\infty$, we have to conclude that $\tilde{k}''_\infty$ is a real strictly negative number and consequently the electromagnetic field does diverge exponentially at infinity and the coefficient of this divergence (the smallest Γ satisfying the aforementioned condition (c) in Definition 2) is linked precisely with the imaginary part of the propagation constant β. From both theoretical and practical points of view, the non-finiteness of energy of the electromagnetic field leads to dramatic consequences. And especially when dealing with the weak form of Maxwell equations: the field does not vanish at infinity. Last, the real part of β is of the same magnitude as $k_0 = \omega/c$ whereas its imaginary part can be extraordinary smaller, say $10^{-8}\ k_0$ in the following numerical experiments and sometimes for very low leakage as small as $10^{-15}\ k_0$! And for experimental reasons this latest information is of prime importance.

2.3 Finite element method and PML

2.3.1 Circular PMLs. In the finite element analysis of wave problems in open space, one of the main difficulties is to truncate the unbounded domain. A common approach is to surround a finite region of interest with absorbing boundary conditions at finite distance. An alternative to conditions defined on the boundary is to introduce a special layer of finite thickness surrounding the region of interest such that it is non-reflecting and completely absorbing for the waves entering this layer under any incidence. Such regions have been introduced by Berenger (1994) and are called perfectly matched layers (PML). Nowadays, the most natural way to introduce PML is to consider them as maps on a complex space (Lassas *et al.*, 2001; Lassas and Somersalo, 2001) so that the corresponding change of (complex) co-ordinates leads to equivalent ε and μ (that are complex, anisotropic, and inhomogeneous even if the original ones where real, isotropic, and homogeneous). This leads automatically to an equivalent medium with the same impedance than the one of the initial ambient medium since ε and μ are transformed in the same way and this ensures that the interface with the layer is non-reflecting. Moreover, a correct choice of the complex map leads to an absorbing medium able to dissipate the outgoing waves. The problem can therefore be properly truncated under the condition that the artificial boundary is situated in a region where the field is damped to a negligible value. To sum up, we have a problem in an unbounded region with outgoing propagating waves or with exponentially diverging waves. A change of co-ordinates is performed such that it corresponds to the identity map in a region of

interest (bounded, convex and, for all practical purposes, with a simple shape) and to complex co-ordinates for the surrounding region. These complex co-ordinates are chosen to turn propagating waves to evanescent waves (i.e. exponentially decreasing at infinity) so that this outer domain can be truncated.

The geometry of most MOF leads to rather use cylindrical PML. In this case, the PML corresponds to a complex stretch of the radial co-ordinate ρ, the region of interest is a disk defined by $\rho < R^*$ and the PML region is a circular annulus around the region of interest defined by $R^* < \rho < R^{\text{trunc}}$. R^* and R^{trunc} are real constants. As the expressions of the material tensors in Cartesian co-ordinates are needed, the whole setting requires a transformation between Cartesian and cylindrical co-ordinates. The recipe involves a sequence of co-ordinate systems. We start here with the physical coordinates and we finish with the modelling co-ordinates. The mapping will therefore be from the last system of the list to the first one while the pull back maps will be from the first system to the last one.

(1) (x, y, z) are real valued classical Cartesian co-ordinates.

(2) $(\tilde{x}, \tilde{y}, \tilde{z})$ are a complex stretch of the previous Cartesian co-ordinates. They are complex valued and it is fundamental to understand that this change is an active transformation rather than a mere change of co-ordinates in the sense that the ambient space is changed. (x, y, z) are a parametrization of $\mathbb{R}^3$ and the complex stretch corresponds to an extension of the problem to $\mathbb{C}^3$ and more precisely to a three dimensional subspace Γ of $\mathbb{C}^3$ (in terms of real dimensions $\mathbb{C}^3$ is six dimensional and $\mathbb{R}^3$ and Γ are three dimensional) (Lassas *et al.*, 2001; Lassas and Somersalo, 2001). The map from Γ to $\mathbb{R}^3$ is chosen in such a way that the restriction of this map to the region of interest is the identity map. The solution of the original problem on $\mathbb{R}^3$ can be extended analytically to $\mathbb{C}^3$ and then restricted to Γ. If the complex stretch is correctly chosen, this "complexified" solution on Γ is evanescent where the physical solution involves outgoing or even exponentially diverging waves.

(3) $(\tilde{\rho}, \tilde{\theta}, \tilde{z})$ is a cylindrical representation of $(\tilde{x}, \tilde{y}, \tilde{z})$.

(4) (ρ_c, θ_c, z_c) are real-valued cylindrical co-ordinates on Γ. They are related to $(\tilde{\rho}, \tilde{\theta}, \tilde{z})$ via $\tilde{\theta} = \theta_c$, $\tilde{z} = z_c$, and a radial complex stretch:

$$\tilde{\rho} = \int_0^{\rho_c} s_\rho(\rho')\mathrm{d}\rho', \tag{11}$$

where s_ρ is a complex-valued function of a real variable, i.e. $s_\rho = 1$ in the central region of interest defined by $\rho_c < R^*$ (the complex stretch corresponds to an identity map in this region) and s_ρ has a complex value in the PML defined by $R^* < \rho < R^{\text{trunc}}$.

(5) (x_c, y_c, z_c) are the Cartesian representation of (ρ_c, θ_c, z_c) and are also real-valued co-ordinates that will be called modelling co-ordinates. This is the modelling space where the numerical approximations are written, where the finite element mesh is defined, and where all the outgoing waves are turned to evanescent ones so that the computation domain can be truncated.

In the end, only the real-valued co-ordinates x, y, z and x_c, y_c, z_c are involved but the complex map corresponds to a complex valued Jacobian. In the case of cylindrical

coordinates, $\tilde{\rho}$ and ρ_c are just introduced to compute the radial stretch. Note also that $\theta_c = \tilde{\theta}$ and therefore will be simply denoted θ. The Cartesian to cylindrical co-ordinates transformation is just used to obtain the Cartesian expression of the corresponding metric tensor. The Jacobian associated to these changes of co-ordinates are:

$$J_{\tilde{x}\tilde{\rho}} = J_{x\rho}(\tilde{\rho}, \theta),\ J_{\tilde{\rho}\rho c} = \mathrm{diag}((\partial\tilde{\rho}/\partial\rho_c), 1, 1) = \mathrm{diag}\,(s_\rho(\rho_c), 1, 1),\ J_{\rho_c x_c}$$
$$= J_{\rho x}(\rho_c(x_c, y_c), \theta(x_c, y_c)).$$

The global Jacobian J_s is the product of the individual Jacobians:

$$J_s = J_{\tilde{x}\rho} J_{\tilde{\rho}\rho_c} J_{\rho_c x_c} = \mathbf{R}(\theta)\,\mathrm{diag}\left(s_\rho, \frac{\tilde{\rho}}{\rho_c}, 1\right)\mathbf{R}(-\theta), \tag{12}$$

where $\mathbf{R}(\theta)$ denotes the following matrix of rotation:

$$\mathbf{R}(\theta) = \begin{pmatrix} \cos\theta & -\sin\theta & 0 \\ \sin\theta & \cos\theta & 0 \\ 0 & 0 & 1 \end{pmatrix}.$$

Note that we solve in fact numerically the extended problem obtained by the complex stretch equation (11) and defined on Γ that has the very remarkable property to coincide with our original problem in the region of interest. In order to comply with traditional notation in the PML context and to avoid cumbersome notations, we drop the c subscript associated with the modelling co-ordinates that will subsequently be denoted as ρ and (x, y, z) without any ambiguity. For isotropic uniform media outside the region of interest, the cylindrical PML characteristics are obtained by multiplying ε and μ by the following complex matrix:

$$\mathbf{T}_s^{-1} = J_s^{-1} J_s^{-\mathrm{T}} \det(J_s) = \mathbf{R}(\theta)\mathrm{diag}\left(\frac{\tilde{\rho}}{s_\rho\rho}, \frac{s_\rho\rho}{\tilde{\rho}}, \frac{s_\rho\tilde{\rho}}{\rho}\right)\mathbf{R}(-\theta) =$$

$$\begin{pmatrix} ((\rho s_\rho \sin(\theta)^2)/\tilde{\rho}) + ((\tilde{\rho}\cos(\theta)^2)/\rho s_\rho) & \sin(\theta)\cos(\theta)((\tilde{\rho}/\rho s_\rho) - (\rho s_\rho/\tilde{\rho})) & 0 \\ \sin(\theta)\cos(\theta)((\tilde{\rho}/\rho s_\rho) - (\rho s_\rho/\tilde{\rho})) & ((\rho s_\rho \cos(\theta)^2)/\tilde{\rho}) + ((\tilde{\rho}\sin(\theta)^2)/\rho s_\rho) & 0 \\ 0 & 0 & \tilde{\rho} s_\rho/\rho \end{pmatrix}.$$

This latest expression is the metric tensor in Cartesian co-ordinates (x, y, z) for the cylindrical PML and θ, ρ, $\tilde{\rho}$, and $s_\rho(\rho)$ are explicit functions of the variables x and y. Another remarkable property of the PML is that they provide the correct extension to non-Hermitian operators (since $\mathbf{T}_s$ is complex and symmetric) that allow the computation of the leaky modes and this may be obtained via a correct choice of the PML parameters, namely R^*, R^{trunc}, and $s_\rho(\rho)$. The method used to compute these parameters is accurately described hereunder (Figure 1).

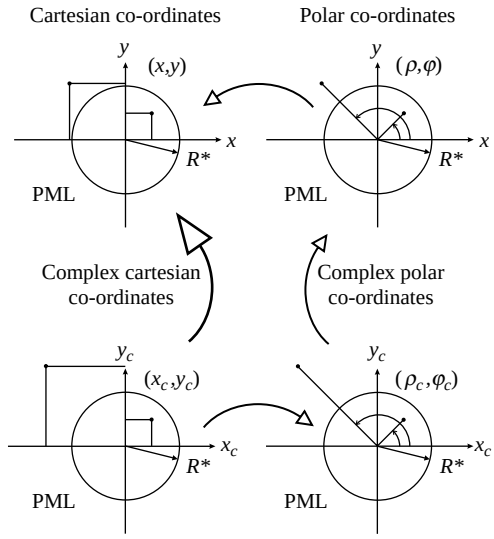

Notes : The *physical space* in Cartesian (x,y) and polar (ρ,φ) co-ordinates are linked by $x = \rho \cos \varphi$ and $y = \rho \sin \varphi$. The stretched complex polar co-ordinates (ρ_c,φ_c) and the real polar co-ordinates are linked by $\rho = \int_0^{\rho_c} s_\rho(\rho')\, d\rho'$ (where s_ρ is a complex valued function) and $\varphi = \varphi_c$. Finally, the complex Cartesian co-ordinates which characterizes the *modelling space* and the complex polar co-ordinates are linked by $\rho_c = \sqrt{x_c^2 + y_c^2}$ and $\varphi_c = 2 \arctan\left(\frac{y_c}{x_c + \sqrt{x_c^2 + y_c^2}}\right)$

Figure 1.
Four different systems of co-ordinates in order to obtain circular PML

2.3.2 How to choose the complex stretch coefficient?. For this purpose, we first introduce new tensor fields $\underline{\underline{\varepsilon}}_s(x,y)$ and $\underline{\underline{\mu}}_s(x,y)$ defined as follows:

$$\underline{\underline{\zeta}}_s := \mathrm{J}_s^{-1}\, \underline{\underline{\zeta}}_r\, \mathrm{J}_s^{-T} \det(\mathrm{J}_s) \quad \text{for } \zeta = \{\varepsilon, \mu\}, \tag{13}$$

We are now in a position to introduce a new electromagnetic field (called substituted field in the sequel) $F_s = (H_s, E_s)^{\mathrm{T}}$ which is solution of equation (2) except that we have replaced $\underline{\underline{\varepsilon}}_r$ and $\underline{\underline{\mu}}_r$ by $\underline{\underline{\varepsilon}}_s$ and $\underline{\underline{\mu}}_s$. The main feature of this latest field is the remarkable correspondence with the first field F; whichever the function s_ρ provided that it equals 1 for $\rho < R^*$, the two fields F and F_s are identical in the region $\rho < R^*$ (Berenger, 1994). In other words, the PML is completely reflectionless. In addition, for complex valued functions s_ρ ($\Im m\{s_\rho\}$ strictly positive in PML), the field F_s may converge exponentially towards zero although its counterpart F diverges exponentially: F_s is of

finite energy and for this substituted field a weak formulation can be easily derived which is essential when dealing with finite element method.

Moreover, when dealing with simple stretched functions it is possible to give a simple criterion which ensures the exponential decreasing of the field F_s. For instance, take the following example:

$$s_\rho(\rho') = \begin{cases} 1 & \text{for } \rho' \leq R^* \\ \xi & \text{in PML} \end{cases}$$

where ξ is a complex number. In that case, the complex function $\rho(\rho_c)$ is given by:

$$\rho = \begin{cases} \rho_c & \text{for } \rho_c \leq R^* \\ R^* + \xi(\rho_c - R^*) & \text{in PML} \end{cases}$$

The function U can be reexpressed in the stretched polar co-ordinates in the PML as per:

$$U_{\text{cs}}(\rho_c, \varphi_c) = \sum_{n \in \mathbb{Z}} c_n H_n^{(1)}\left(\tilde{k}_\infty(R^* + \xi(\rho_c - R^*))\right) e^{in\varphi_c}.$$

For large values of ρ_c, the behaviour of U_{cs} is governed by $\exp\left(i\tilde{k}_\infty(R^* + \xi(\rho_c - R^*))\right)$ which exponentially converges towards zero if $\tilde{k}_\infty \xi$ has a strictly negative imaginary part. Consequently, the field F_s converges exponentially towards zero as well (and therefore is of finite energy) if the simple following criterion is fulfilled:

$$\gamma := \tilde{k}''_\infty \xi' + \tilde{k}'_\infty \xi'' > 0. \tag{14}$$

Keeping in mind that $\tilde{k}''_\infty$ is negative whereas $\tilde{k}'_\infty$ is positive, a straightforward solution could be $\xi' < 0$ and $\xi'' = 0$. In other words, ξ would be a real negative number. But, in that case, the function $\rho(\rho_c)$ is no longer monotonic and therefore we are "doomed" to choose the number ξ within the upper complex plane. As a conclusion, for a given couple (k_0, β) in $\mathbb{R}^+ \times \mathbb{C}^+$, we compute $\tilde{k}_\infty$, from equation (10) and ξ is chosen in such a way that γ is sufficiently large in order to ensure that the skin layer thickness of the substituted electromagnetic field is of the same order than the thickness of the PML (Figure 2).

In order to illustrate the decreasing of the substituted field within the PML, let us consider a six hole MOF shown in Figure 3. The Figure 2 shows the exponential decreasing of the z component of the electric field for a parameter $\xi = 1 - 2i$ and for a wavelength $\lambda = 1.55\ \mu$m: we find $\beta = 5.8323 \times 10^5 + 0.173092\, i\ \text{m}^{-1}$. The decreasing of the field which is characterized by γ is therefore computed by two different ways: The first one (denoted γ_{th}) through the equation (14) and the second one (denoted γ_{num}), by numerical computing of the field itself. Finally, we find $\gamma_{\text{th}} = 4.9810^5\ \text{m}^{-1}$ and $\gamma_{\text{num}} = 4.97 \times 10^5\ \text{m}^{-1}$.

2.3.3 Weak formulation for the substituted field F_s. If ξ verifies the inequality (14) the field converges towards zero at infinity and, as a result, a weak formulation can be easily derived. For instance, with the electric field E_s, we obtain:

$$\int_{\mathbb{R}^2} (\underline{\underline{\mu_s}}^{-1} \operatorname{curl}_\beta \times E_s) \cdot \overline{(\operatorname{curl}_{\bar{\beta}} \times E_s^*)} \mathrm{d}x\mathrm{d}y - \quad k_0^2 \int_{\mathbb{R}^2} (\underline{\underline{\varepsilon_s}} E_s) \cdot \bar{E}_s^* \, \mathrm{d}x\mathrm{d}y = 0 \tag{15}$$

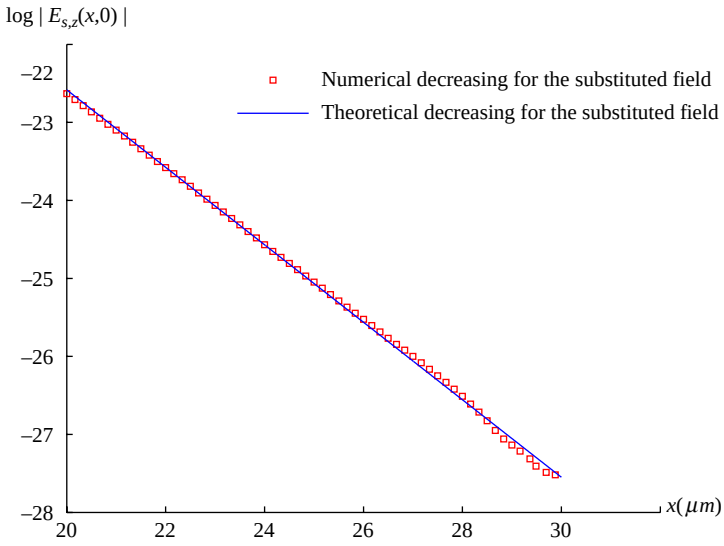

Figure 2.
Behaviour of the substituted field within the PML

Notes : The logarithm of the z component of the substituted electric field, log | $E_{s,z}(x,0)$ |, is plotted versus x in the PML (for $R^* < x < R^{trunc}$). The structure is depicted in Fig. 3

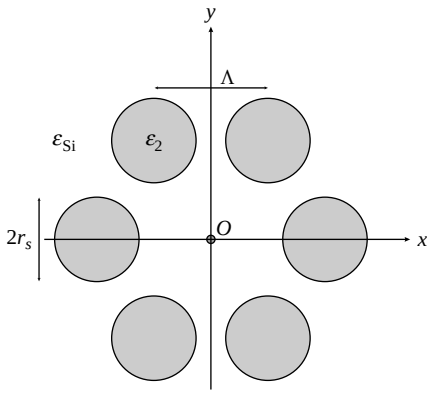

Figure 3.
Six hole MOF structure

Notes : A bulk of silica is drilled by six air holes distant each other from $\Lambda = 6.75\ \mu m$. Each hole is circular with a radius equal to $r_s = 2.5\ \mu m$. Note that for such as structure no propagating mode can propagate

for any test function E_s^*. Then, we split the electric field E_s into a transverse part E_t and a longitudinal part E_z:

$$E_s = E_t + E_z\hat{z}$$

from which, we are led to:

$$\mathrm{curl}_\beta \times E_s = i\beta E_t \times \hat{z} + \nabla_t E_z \times \hat{z} + (\nabla_t \times E_t)\hat{z}.$$

Finally, by letting:

$$\begin{cases} \mathscr{L}_0(E_t) = E_t \times \hat{z} \\ \mathscr{L}_1(E_s) = \nabla_t E_z \times \hat{z} + (\nabla_t \times E_t)\hat{z} \end{cases}$$

we derive the following weak formulation for the substituted electric field:

$$\int_{\mathbb{R}^2} \beta^2 F_0 + i\beta(F_{1,1} + F_{1,2}) + F_2 \,\mathrm{d}x\mathrm{d}y = \int_{\mathbb{R}^2} k_0^2 G \,\mathrm{d}x\mathrm{d}y \tag{16}$$

with:

$$\begin{cases} F_0 = (\underline{\underline{\mu_s}}^{-1}\,\mathscr{L}_0)(E_t)\cdot(\mathscr{L}_0)\left(\overline{E_t^*}\right) \\ F_{1,1} = (\underline{\underline{\mu_s}}^{-1}\,\mathscr{L}_0)(E_t)\cdot(\mathscr{L}_1)\left(\overline{E_s^*}\right) \\ F_{1,2} = (\underline{\underline{\mu_s}}^{-1}\,\mathscr{L}_1)(E_s)\cdot(\mathscr{L}_0)\left(\overline{E_t^*}\right) \\ F_2 = (\underline{\underline{\mu_s}}^{-1}\,\mathscr{L}_1)(E_s)\cdot(\mathscr{L}_1)\left(\overline{E_s^*}\right) \\ G = (\underline{\underline{\varepsilon_s}}E_s)\cdot\vec{E_s^*} \end{cases}$$

In most applications in optics, we have to find the dispersion curves, *i.e.* to look for β's for a given k_0. In such a case, the eigenproblem described in (16) leads to a generalized eigenproblem owing to the presence of both β and β^2 (Tisseur and Meerbergen, 2001, for instance).

2.3.4 Generality on finite elements. The discretisation of the equations is obtained via finite elements (Zolla *et al.*, 2005; Nicolet *et al.*, 2004, 2006; Guenneau *et al.*, 2001, 2002; Lasquellec *et al.*, 2002; Nicolet and Zolla, 2007). The cross-section of the guide is meshed with triangles and Whitney finite elements are used, i.e. edge elements for the transverse field and nodal elements for the longitudinal field:

$$E_t = \sum_{\mathrm{j}=1}^{\#\mathrm{edges}} e_j^t w_e^j(x,y) \text{ and } E_z = \sum_{j=1}^{\#\mathrm{nodes}} e_j^z w_n^j(x,y),$$

where e_j^t denotes the line integral of the transverse component E_t on the edges, e_j^z denotes the line integral of the longitudinal component E_z along one unit of length of the z-axis (which is equivalent to the nodal value), and w_e^j and w_n^j are, respectively, the basis functions of Whitney 1-forms and 0-forms on triangles.

3. Numerical results

3.1 Comparison with the multipole method

One of our former challenge was to compare our results with those obtained with other methods such as the multipole method. The philosophy of this latest method is completely different from those described in this paper and the reader can refer to Zolla *et al.* (2005) for a comprehensive review of this method. This method is indeed well-suited for the step index MOF. Be that as it may, we consider the hexagonal structure shown in Figure 3 for a given wavelength $\lambda_0 = 1.55\ \mu$m for which the index of silica is about $\varepsilon_{Si} = 1.4440$. For this structure, we give a map representing one mode in Figure 3 and the corresponding complex effective index, namely $n_{eff} = \beta/k_0$ for the two different methods: $1.438774 + 4.32 \times 10^{-8}i$ for the multipole method and $1.438773 + 4.28 \times 10^{-8}i$ for the finite element method. Besides, it is worth knowing that the practical implementation of the model has been performed thanks to the COMSOL software with about 40,000 elements and the computation takes a few seconds on an ordinary laptop. Note that regarding its smallness with respect to the real part, the imaginary part is computed with an amazing accuracy.

3.2 Leaky modes for gradient index MOF

In this paragraph, we present some numerical results for more sophisticated fibres. Besides of the six air holes, the permittivity of the bulk varies continuously as per:

$$\varepsilon_r(x,y) = \varepsilon_1 + \varepsilon_1^i \ \exp\left(-\frac{x^2+y^2}{r_0^2}\right) \tag{17}$$

The case corresponding to the precedent paragraph is therefore $\varepsilon_1 = \varepsilon_{Si}$ and $\varepsilon_1^i = 0$. By way of example, we take $r_0 = 10\ \mu$m (r_0 is therefore of the same magnitude as Λ) and we give a curve representing n_{eff} versus ε_1^i with $\varepsilon_1 = \varepsilon_{Si}$ for the same wavelength as before *i.e.* $\lambda_0 = 1.55\ \mu$m. Note that the central symmetry of ε_r does not break the C_{6v} symmetry of the fibre (Figures 4 and 5).

3.3 Leaky modes for elliptical hole MOF

In this paragraph, a six elliptical hole structure is considered as shown in Figure 6 for a given wavelength $\lambda_0 = 1.55\ \mu$m for which the index of silica is about $\varepsilon_{Si} = 1.4440$. The elliptical holes are distant from each other from $\Lambda = 6.75\ \mu$m and are characterized by their semi-major axis a and their semi-minor axis b. Moreover, the orientation and the choice of a and b are chosen in such a way that both the C_{6v} structure and the area of these ellipses are preserved ($ab = r_0^2$). Eventually, for $r_0 = 2.5\ \mu$m, and for different values of b, effective indices (real part in Figure 7 and imaginary part in Figure 8) are given.

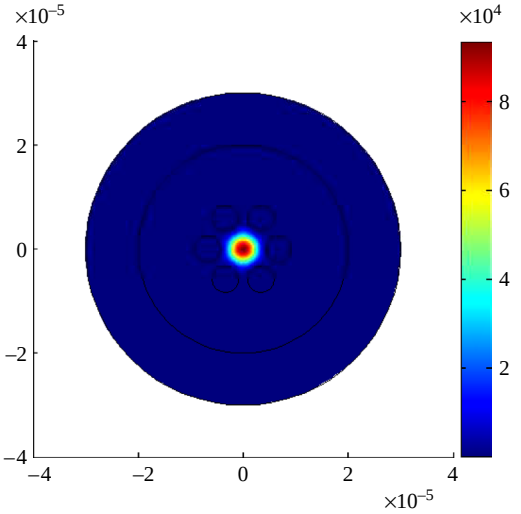

Figure 4.
Modulus of the Poynting vector for the C_{6v} six hole MOF shown in Figure 3

Note : The structure is surrounded by cylindrical PML

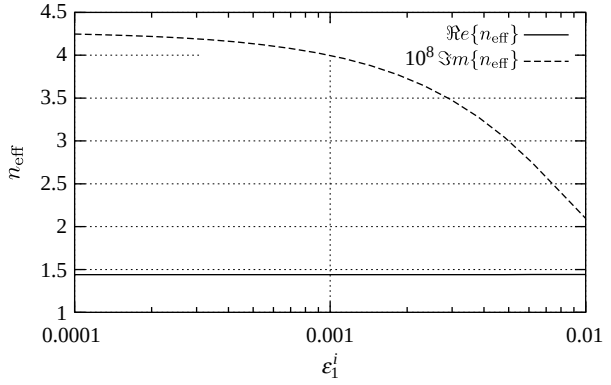

Figure 5.
The complex effective index n_{eff} as a function of ε_1^i

4. Conclusion

The search for leaky modes is far from being a simple task. The first way of obtaining these modes consists in computing the scattering matrix and looking for poles of this latest matrix in the complex plane. This numerical stage is a delicate operation and has two major drawbacks: the "pole hunting" in the complex plane is generally performed in a point-by-point fashion and this method is merely devoted to step index fibres. On the other hand, the method used in this paper as shown before is a versatile and efficient method and may be useful for obtaining leaky modes in delicate situations. Finally, we hope to obtain leaky modes for the challenging nonlinear MOFs.

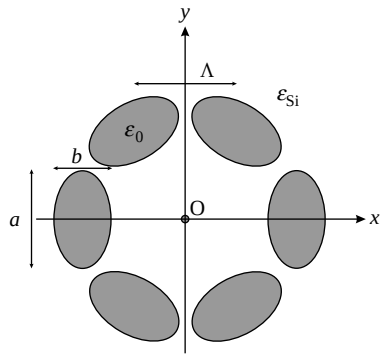

Note : The $C_{6\upsilon}$ structure is preserved

Figure 6.
Six elliptical hole MOF structure

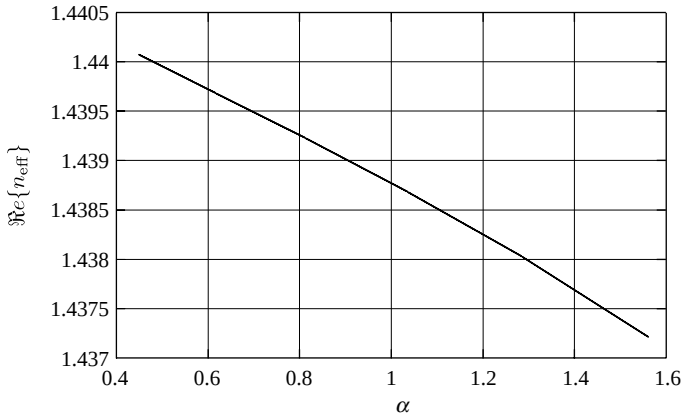

Figure 7.
Real part of effective index versus the parameter $\alpha = b/a$

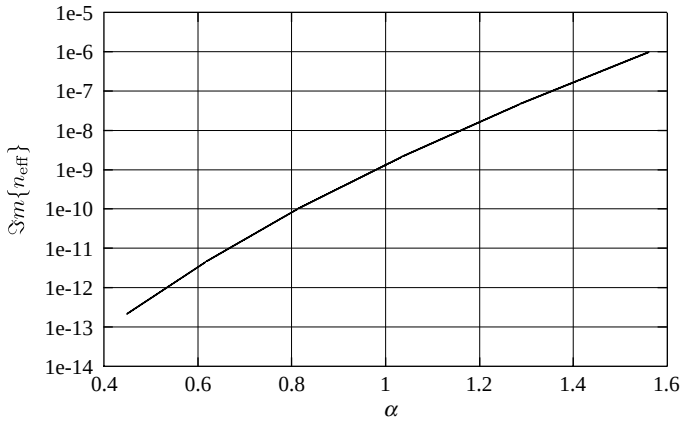

Note : For the value $\alpha = 0.44$ (Ellipses are close to touching) leakage is extremely weak $\Im m\{n_{\text{eff}}\} = 5.10^{-13}$!!

Figure 8.
Imaginary part of effective index versus the parameter $\alpha = b/a$

References

Berenger, J-P. (1994), "A perfectly matched layer for the absorption of electromagnetic waves", *Journal of Computational Physics*, Vol. 114, pp. 185-200.

Cregan, R.F., Mangan, B.J., Knight, J.C., Birks, T.A., Russell, P.S., Roberts, P.J. and Allan, D.C. (1999), "Single-mode photonic band gap guidance of light in air", *Science*, Vol. 285, pp. 1537-9.

Guenneau, S., Nicolet, A., Zolla, F. and Lasquellec, S. (2002), "Modeling of photonic crystal optical fibers with finite elements", *IEEE Transactions on Magnetics*, Vol. 38 No. 2, pp. 1261-4.

Guenneau, S., Nicolet, A., Zolla, F., Geuzaine, C. and Meys, B. (2001), "A finite element formulation for spectral problems in optical fibers", *COMPEL*, Vol. 20 No. 1, pp. 120-31.

Guenneau, S., Lasquellec, S., Nicolet, A. and Zolla, F. (2002), "Design of photonic band gap optical fibers using finite elements", *COMPEL*, Vol. 21 No. 4, pp. 534-9.

Lassas, M. and Somersalo, E. (2001), "Analysis of the PML equations in general convex geometry", *Proceedings of the Royal Society of Edinburgh*, Vol. 131 No. 5, pp. 1183-207.

Lassas, M., Liukkonen, J. and Somersalo, E. (2001), "Complex Riemannian metric and absorbing boundary condition", *Journal de Mathematiques Pures et Appliquees*, Vol. 80 No. 7, pp. 739-68.

Nicolet, A. and Zolla, F. (2007), "Finite element analysis of helicoidal waveguides", *IET Science, Measurement & Technology*, Vol. 1 No. 1, pp. 67-70.

Nicolet, A., Zolla, F. and Guenneau, S. (2004), "Modelling of twisted optical waveguides with edge elements", *The European Physical Journal-Applied Physics*, Vol. 28 No. 5, pp. 153-7.

Nicolet, A., Movchan, A.B., Guenneau, S. and Zolla, F. (2006), "Asymptotic modelling of weakly twisted electrostatic problems", *Comptes Rendus Mécanique*, Vol. 334 No. 2, pp. 91-7.

Ranka, J.K., Windeler, R.S. and Stentz, A.J. (2000), "Visible continuum generation in air-silica microstructured optical fibers with anomalous dispersion at 800 nm", *Opt. Lett.*, Vol. 25, pp. 25-7.

Tisseur, F. and Meerbergen, K. (2001), "The quadratic eigenvalue problem", *Siam Review*, Vol. 43 No. 2, pp. 235-86.

Zolla, F., Renversez, G., Nicolet, A., Kuhlmey, B., Guenneau, S. and Felbacq, D. (2005), *Foundations in Photonic Crystal Fibres*, Imperial College Press, London.

About the authors

Y. Ould Agha was born in Nouakchott, Mauritania, on the 31st December 1977. He obtained the Master in Electronics, Power Systems and Automatics from Nouakchott University in 2002. In July 2004, he received the Master of Research in Components and Systems for the data processing, at the University of Blaise Pascal (Clermont-Ferrand-France). He is currently a PhD student in Physics at the Fresnel Institute (University of Provence). E-mail: yacoub.ould-agha@fresnel.fr

F. Zolla received a PhD thesis on Electromagnetic Diffraction at the University of Marseille in 1993. He is currently a Professor at the University of Provence and is the author of many papers on theoretical and numerical study of gratings, photonic crystals and homogenization of Maxwell equations. An emerging research topic is that of spectral analysis of dielectric waveguides and numerical schemes for the modelling of exotic materials such as Photonic Crystal Fibers, Twisted Fibers, and Invisibility Cloaks. F. Zolla is the corresponding author and can be contacted at: frederic.zolla@fresnel.fr

A. Nicolet has received his Engineering Degree (Ingénieur Civil Electricien (Electronique)) in 1984 and his PhD in Applied Sciences in 1991 both from the University of Liège, Belgium.

From 1984 to 1994, he was a Research Engineer at the Department of Applied Electricity of the University of Liège. From 1994 to 1996, he was the Head of the Department of Electrical Engineering and Power Electronics of the Ecole Supérieure des Ingénieurs de Marseille(ESIM) France. In 1996, he received the "Habilitation à Diriger des Recherches" from the University Paul Cézanne of Aix-Marseille III. Since, 1996, he is a Professor at the University Paul Cézanne of Aix-Marseille III (63rd section: electronics, optronics and systems) and he has joined the Fresnel Institute (UMR CNRS 6133) at his creation in 2000. His main research interests are the numerical computations of electromagnetic fields and he presently focuses on the modelling of micro-structured optical fibres. He is author or co-author of more than 80 papers and of a book entitled *Foundations of Photonic Crystal Fibres* (Zolla, Renversez, Nicolet & al., Imperial College Press, 2005). E-mail: andre.nicolet@fresnel.fr

S. Guenneau graduated with a PhD thesis on Models of Photonics from University of Aix-Marseille in 2001. He subsequently worked as a Research Assistant in 2001-2004 with Professor Alexander Movchan at Liverpool University and Sir John Pendry at Imperial College London. He was then appointed as an Applied Mathematics Lecturer in 2004 at Liverpool University. In January 2006, he took over a Research Scientist position at Fresnel Institute (Marseille) within the Centre National de la Recherche Scientifique (CNRS) E-mail: sebastien.guenneau@fresnel.fr